biomedicines

MDPI

Article

Moxibustion Alleviates Ferroptosis-Associated Alterations and Promotes the Recovery of Gastrointestinal Function in a Mouse Model of Postoperative Ileus

Fenglin Mei [1,2,†], Shufan Zhang [2,†], Yujuan Zhang [2], Jingjing Shen [2], Fangfang Zhao [1,*] and Chengcai Kong [1,3,*]

[1] School of Nursing and Rehabilitation, Nantong University, Nantong 226000, China; phy_lin@163.com
[2] The Affiliated Changzhou NO.2 People's Hospital of Nanjing Medical University, Changzhou 213000, China; zhangshufan9911@163.com (S.Z.); 13861267919@163.com (Y.Z.); 18360428861@163.com (J.S.)
[3] Changzhou Maternal and Child Health Care Hospital, Changzhou Medical Center, Nanjing Medical University, Changzhou 213000, China
* Correspondence: moonstar148@hotmail.com (F.Z.); kongchengcai12@163.com (C.K.)
† These authors contributed equally to this work.

Abstract

Background/Objectives: Postoperative ileus (POI) is a common complication after abdominal surgery with limited effective therapeutic options. **Methods:** We first performed transcriptomic screening of publicly available intestinal manipulation (IM)/POI-related datasets (GSE134942, GSE164909, and GSE263125) using signature scoring, differential expression, and pathway enrichment with cross-cohort validation. We then evaluated moxibustion at Shenque (CV8) in an IM-induced POI mouse model. Mice were randomized into Sham, POI, MOX, and POI + MOX groups; moxibustion (1.5 cm distance, 20 min/day) was applied for 4 weeks. Gastrointestinal transit was assessed by FITC-dextran, intestinal injury by H&E staining, inflammatory mediators by ELISA (COX-2, IL-1β, IL-6, TNF-α), barrier markers by ZO-1 and occludin expression (qRT-PCR, immunoblotting, immunohistochemistry), and ferroptosis-related alterations by MDA, Fe^{2+}, GSH and GPX4. **Results:** Transcriptomic screening consistently highlighted inflammation activation and barrier suppression after IM and nominated ferroptosis-associated remodeling as a reproducible feature across independent mouse cohorts with directional concordance in a human surgical dataset. Moxibustion improved transit, attenuated intestinal injury, reduced COX-2 and pro-inflammatory cytokines, partially restored ZO-1 and occludin, and alleviated a pro-ferroptotic state by lowering MDA and Fe^{2+}, increasing GSH, and upregulating GPX4. **Conclusions:** These results indicate that ferroptosis emerged from public-data screening and that moxibustion promotes POI recovery, at least in part, by counteracting an IM-associated inflammation-barrier impairment-ferroptosis axis.

Keywords: gastrointestinal motility; moxibustion; postoperative ileus; Shenque acupoint; ferroptosis

Check for updates

Academic Editor: Hengrui Liu

Received: 18 May 2026
Revised: 29 September 2026
Accepted: 15 October 2026
Published: 30 October 2026

Copyright: © 2026 by the authors. Licensee MDPI, Basel, Switzerland. This article is an open access article distributed under the terms and conditions of the Creative Commons Attribution (CC BY) license.

1. Introduction

Postoperative ileus (POI) is a prevalent complication after abdominal surgery, characterized by transient but clinically meaningful dysmotility of the gastrointestinal tract (GIT) [1,2]. Patients often experience substantial discomfort and increased morbidity, resulting in prolonged hospitalization and an increased socio-economic burden [3]. Accumulating evidence indicates that postoperative hypomotility promotes intestinal stasis and

bacterial overgrowth, which can trigger and amplify a complex inflammatory response [4]. Excessive release of pro-inflammatory cytokines activates resident immune populations and enteric glia, thereby aggravating local inflammation and, importantly, further impairing epithelial barrier integrity [5]. Although inflammation and barrier disruption are increasingly recognized as central features of POI, the upstream molecular programs that coordinate these pathological processes—and thus represent actionable therapeutic targets—remain incompletely defined.

Ferroptosis is a regulated, non-apoptotic cell death process driven by iron-dependent lipid peroxidation and antioxidant system failure, typically involving glutathione (GSH) depletion and compromised lipid peroxide detoxification [6,7]. Ferroptosis has been implicated in intestinal inflammatory diseases such as ulcerative colitis and Crohn's disease, where oxidative injury and epithelial dysfunction contribute to barrier breakdown [8]. However, whether ferroptosis-related programs participate in POI has not been systematically evaluated, and mechanistic studies in POI remain limited. To address this knowledge gap and to avoid a purely hypothesis-driven, post hoc mechanistic narrative, we conducted a systematic screening of publicly available transcriptomic datasets relevant to intestinal manipulation (IM)/POI [9–11]. Across a time-course IM dataset (Control→IM3h→IM24h), we identified a coordinated transcriptional shift characterized by inflammation activation, suppression of barrier/tight-junction programs, and a prominent ferroptosis-associated remodeling over time. This ferroptosis-associated signal was further supported in an independent mouse cohort (sham surgery vs. IM) and showed directional concordance in human intraoperative intestinal samples, highlighting ferroptosis as a clinically relevant candidate mechanism rather than a dataset-specific artifact. These multi-cohort observations constitute a key premise of the present study and provide a rationale for targeted in vivo validation of ferroptosis alongside inflammation and barrier dysfunction in POI.

Traditional Chinese medicine (TCM) has been widely used for centuries to treat gastrointestinal disorders, including postoperative dysmotility. For example, Shenhuang Plaster has been reported to promote recovery of gastrointestinal transit in a postoperative ileus rat model [12]. Moxibustion, a common TCM intervention, delivers localized thermal stimulation by burning moxa over specific acupoints and has been proposed to modulate inflammatory and functional outcomes in multiple conditions [13,14]. Recent work suggests that moxibustion may ameliorate Crohn's disease-associated intestinal fibrosis through regulation of signaling pathways involved in intestinal tissue responses [15,16]. However, little is known about whether moxibustion benefits POI, and more importantly, whether it can modulate the IM-associated inflammation-barrier-ferroptosis program highlighted by our public dataset screening.

Thus, the aim of the present study was to investigate the multi-factorial effects of moxibustion at the Shenque (CV8) acupoint on gastrointestinal transit, intestinal histopathology, pro-inflammatory cytokine production, epithelial barrier integrity, and ferroptosis-related alterations in an IM-induced mouse model of POI. By integrating public multi-cohort transcriptomic screening with targeted experimental validation, we sought to establish a coherent mechanistic framework in which ferroptosis-associated remodeling links postoperative inflammation and barrier dysfunction and is amenable to modulation by moxibustion.

2. Materials and Methods

2.1. Preparations of Animals

All experimental procedures complied with the ARRIVE guidelines and were performed in accordance with procedures approved by the Laboratory Animal Welfare and Ethics Committee of Nanjing Medical University (Approval No. IACUC-2211079). Male Institute of Cancer Research (ICR) mice, aged 8–10 weeks and weighing 20–25 g, were

obtained from Cavens Laboratory Animal Technology Co., Ltd. (Changzhou, China). After arrival, the mice were acclimatized to the animal facility for 7 days before any experimental procedure. Animals were maintained under controlled laboratory conditions at 22 ± 2 °C and 40–60% relative humidity with a 12-h light/dark cycle. An irradiated maintenance diet for SPF laboratory mice (XTI01WC-009, Jiangsu Xietong Pharmaceutical Bioengineering Co., Ltd., Nanjing, China), containing ≥18% crude protein, ≥4% crude fat, ≤5% crude fiber, and ≤8% crude ash, was provided ad libitum together with tap water, except during the specified pre-experimental fasting periods.

2.2. Mice Surgery and Moxibustion

The 48 experimental mice (12 mice each group) were randomly and evenly allocated into the sham group (Sham), postoperative ileus group (POI), moxibustion group (MOX), and postoperative ileus + moxibustion group (POI + MOX). After overnight fast, all mice were operated under anesthesia with pentobarbital sodium solution (1%, 50 mg/kg, i.p.).

POI was induced in ICR mice by intestinal manipulation (IM) as described previously [17]. Following adequate anesthesia, a midline laparotomy was performed. The small intestine was gently exteriorized onto sterile gauze moistened with warm saline and manipulated along its entire length using two moistened cotton applicators. The intestine was subsequently returned to the abdominal cavity, and the abdominal wall and skin were closed in two layers. Mice in the Sham and MOX groups underwent laparotomy without intestinal manipulation.

After the experimental POI mice models were successfully established, and following a 24-h post-operative recovery period (designated as Day 1), the MOX and POI + MOX groups were given their treatment intervention. After fixation on the frame, the Shenque (CV8) acupoint located at the mice's navel was chosen in the MOX and POI + MOX groups. A special animal-specific moxa stick (diameter 0.5 cm, height 0.5 cm, "Han Medicine", Nanyang, China) was ignited and hung 1.5 cm above Shenque (CV8) acupoint for treatment 20 min once daily for 4 weeks (from Day 1 to Day 28, representing a prolonged post-acute intervention window). The Sham and POI groups were only immobilized on the identical frame daily for 20 min to equalize any potential handling- or restraint-induced stress without receiving any additional treatment.

After treatment, all mice were completely anesthetized with pentobarbital sodium (100 mg/kg, i.p.) to finish the below studies and euthanized by cervical dislocation. Six mice per group were randomly allocated to gastrointestinal transit analysis. The remaining six mice per group were used for blood and tissue collection. A distal ileal segment located approximately 5 cm proximal to the ileocecal junction was used as the standardized intestinal sampling region. A 1-cm segment was fixed for H&E staining and immunohistochemistry, whereas adjacent full-thickness distal ileal tissues were snap-frozen for qRT-PCR, Western blotting, and MDA, GSH, and Fe^{2+} assays.

2.3. Data Acquisition and Preprocessing

Three publicly available transcriptomic datasets relevant to intestinal manipulation (IM) and postoperative intestinal dysfunction were obtained from the Gene Expression Omnibus (GEO) database: GSE134942, GSE164909, and GSE263125. Expression data and sample annotations were imported and organized in R version 4.5.2 using GEOquery version 2.78.0.

GSE134942 was used as the discovery time-course dataset. Nine mouse samples were included: Control (n = 3), IM3h (n = 3), and IM24h (n = 3). Gene-level raw counts were used for differential expression analysis. Genes with a raw count of ≥10 in at least three samples were retained. The filtered count matrix was used directly as input for

DESeq2 and was not log2-transformed or externally normalized before differential expression modeling. For sample-level functional scoring, heatmap generation, and expression visualization, the count data were variance-stabilized using the DESeq2 vst function with blind = FALSE.

GSE164909 was used as an independent mouse validation dataset. Only the sham surgery (SS; $n = 3$) and intestinal manipulation (IM; $n = 3$) samples were included in the present analysis. Gene-level raw counts were assembled into a gene-by-sample count matrix. The same filtering criterion used for GSE134942 was applied, retaining genes with a raw count of $\geq$10 in at least three samples. Untransformed counts were used for DESeq2 analysis, whereas variance-stabilized values generated using vst(. . ., blind = FALSE) were used for sample-level scoring and visualization.

For GSE263125, only the human Early/Late surgical subset was included. The analysis comprised eight jejunal muscularis externa samples obtained at Early ($n = 4$) and Late ($n = 4$) intraoperative stages. The GEO-provided normalized matrix, GSE263125_Human_Partek_Early_Late_2_Normalization_Normalized_counts.txt.gz, was used. Expression values were transformed as log2(x + 1) before sample-level functional scoring, heatmap generation, and visualization. Early and Late sample identities were assigned according to the GEO metadata. Differential expression of this paired human dataset was performed separately as described in Section 2.4.

Before downstream analyses, gene identifiers were converted to official species-specific gene symbols. Genes without valid gene-symbol annotation were excluded. When multiple entries mapped to the same gene symbol, the entry with the highest mean expression across the analyzed samples was retained.

2.4. Differential Expression Analysis

Differential expression analyses were performed in R version 4.5.2 within the Bioconductor 3.22 environment. For the mouse RNA-seq datasets GSE134942 and GSE164909, differential expression was analyzed using DESeq2 version 1.50.2 based on the filtered raw count matrices described in Section 2.3. DESeq2 size-factor normalization and negative-binomial generalized linear modeling were applied.

For GSE134942, the design formula was specified as ~ group, and three predefined contrasts were evaluated: IM3h versus Control, IM24h versus Control, and IM24h versus IM3h. For GSE164909, the comparison was IM versus sham surgery (SS). Differential expression significance was assessed using the Wald test, and p values were adjusted for multiple comparisons using the Benjamini–Hochberg method.

For the human GSE263125 dataset, differential expression between the paired Early and Late samples was evaluated using limma version 3.66.0. Expression values were analyzed on the log2-transformed scale described in Section 2.3. Patient identity was included as a blocking factor to account for the paired sampling design, and the Late-versus-Early contrast was evaluated using an empirical Bayes-moderated linear model. p values were adjusted using the Benjamini–Hochberg method.

Unless otherwise specified, genes with adjusted $p < 0.05$ and $|\log2 \text{ fold change}| \geq 1$ were considered significantly differentially expressed.

2.5. Gene Set Construction

Gene sets used for functional analyses were obtained from the Molecular Signatures Database (MSigDB) (https://www.gsea-msigdb.org/, accessed on 29 September 2026). Gene sets from Gene Ontology Biological Process (GOBP) and Kyoto Encyclopedia of Genes and Genomes (KEGG) were primarily selected as reference collections for biological processes related to inflammation, ferroptosis-associated stress, and barrier function. Gene

sets were retrieved using the msigdbr R package (version 25.1.1) in the R statistical environment (v4.5.2) and were organized according to species-specific gene symbols for mouse or human datasets. Functionally related gene sets were further curated and integrated to construct three core functional modules: the inflammation module (Inflammation), the ferroptosis module (Ferroptosis), and the barrier module (Barrier). For biological processes represented by multiple gene sets from different databases with highly overlapping functional annotations, gene sets were merged using a union-based strategy to generate more comprehensive and biologically stable gene collections.

2.6. Enrichment Analysis

Pathway enrichment analyses were performed using clusterProfiler version 4.18.4. For gene set enrichment analysis (GSEA), all genes were ranked using a signed differential-expression statistic. For the mouse datasets, genes were ranked according to the DESeq2 Wald statistic, whereas the limma moderated t statistic was used for the human dataset. GSEA was performed using a weighting exponent of 1, with minimum and maximum gene-set sizes of 10 and 500 genes, respectively. p values were adjusted using the Benjamini–Hochberg method, and pathways with adjusted $p < 0.05$ were considered significantly enriched.

For over-representation analysis (ORA), genes meeting adjusted $p < 0.05$ and $|\log2 \text{ fold change}| \geq 1$ were used as the foreground gene set. The reference universe consisted of all genes retained after the expression-filtering procedures described in Section 2.3. Gene Ontology Biological Process and KEGG pathway enrichment analyses were performed using the enrichGO and enrichKEGG functions, respectively. Species-specific settings were used (organism = "mmu" for mouse and "hsa" for human analyses), and p values were corrected using the Benjamini–Hochberg method.

Sample-level activity of the Inflammation, Ferroptosis, and Barrier modules was evaluated using GSVA version 2.4.9 with the single-sample gene set enrichment analysis (ssGSEA) algorithm. For the mouse datasets, variance-stabilized expression matrices generated as described in Section 2.3 were used as input; for the human dataset, the log2-transformed normalized expression matrix was used. The resulting ssGSEA scores were standardized to z scores separately within each dataset before statistical comparison and visualization.

Enrichment curves and pathway plots were generated using enrichplot version 1.30.0, whereas heatmaps, dot plots, box plots, and other graphical summaries were generated using ggplot2 version 4.0.0 and ggpubr version 0.6.1.

2.7. Quantitative RT-PCR

Total RNA was extracted from intestine tissues using TRIzol reagent (Invitrogen, Carlsbad, CA, USA) according to the manufacturer's instructions. Purified total RNA was reverse transcribed into cDNA using the High-Capacity cDNA Reverse Transcription Kit (Thermo Fisher Scientific, Waltham, MA, USA). qRT-PCR was performed using TB Green Premix Ex Taq II (Tli RNaseH Plus; RR820A, Takara Bio, Kusatsu, Japan) on a MyiQ Single Color Real-Time PCR Detection System (Bio-Rad Laboratories, Hercules, CA, USA). Reactions were performed with an initial denaturation at 95 °C for 30 s, followed by 40 cycles of 95 °C for 5 s and 60 °C for 30 s. Amplification specificity was assessed by melting-curve analysis from 65 °C to 95 °C with 0.5 °C increments and a 5-s acquisition at each step. Each primer pair produced a single dominant melting peak. Relative gene expression was normalized to Gapdh and calculated using the $2^{-\Delta\Delta Ct}$ method. Primer sequences are listed in Table 1, and representative melting curves are provided in Supplementary Figure S1.

Table 1. RT-qPCR primers used in the study.

Gene Symbol	Forward Primer (5′-3′)	Reverse Primer (5′-3′)
ZO-1	GATGTTTATGCGGACGGTGG	CATTGCTGTGCTCTTAGCGG
occludin	AGGTGAATGGGTCACCGAG	AGGCTCCCAAGATAAGCGAAC
GAPDH	GCCGCATCTTCTTTTGCGTC	GAGAACAGTGAGCGCCTAGT

Note: GAPDH was used as an internal control.

2.8. Western Blotting

The intestine tissues were extracted using RIPA lysis buffer containing a protease inhibitor cocktail (Sigma, St. Louis, MO, USA). The total protein concentration was examined using the bicinchoninic acid assay protein concentration assay kit. Equal amounts of total protein were separated on SDS-polyacrylamide gel and transferred to polyvinylidene fluoride membranes (Millipore, Billerica, MA, USA). The membranes were blocked in Tris-buffered saline solution with 5% nonfat milk for 1 h and then hybridized with the following primary antibodies: ZO-1 (1:1000, ab276131, rabbit monoclonal antibody, Abcam, Cambridge, UK), occludin (1:1000, #91131, rabbit monoclonal antibody, Cell Signaling Technology, Danvers, MA, USA), GPX4 (1:1000, 67763-1-Ig, mouse monoclonal antibody, Proteintech, Rosemont, IL, USA) and β-actin (1:5000, 20536-1-AP, rabbit polyclonal antibody, proteintech), followed by incubation with goat anti-rabbit/mouse antibodies. Finally, the ECL reagent was used to detect the protein.

2.9. Hematoxylin and Eosin Staining

At the experimental endpoint, a 1-cm segment of distal ileum located approximately 5 cm proximal to the ileocecal junction was collected from each mouse and fixed in 4% paraformaldehyde at 4 °C for 48 h. Tissues were dehydrated through graded ethanol, cleared in xylene, embedded in paraffin, and cut into 4-μm sections. Three non-consecutive sections separated by approximately 100 μm were examined for each animal (n = 6 animals/group). Five non-overlapping fields per section were evaluated at 200× magnification using a light microscope (Olympus Corporation, Tokyo, Japan). H&E staining was used for qualitative assessment of mucosal architecture and structural injury.

2.10. Immunohistochemical Staining

Intestine tissue sections were deparaffinized, dehydrated, and rehydrated. Then, citrate buffer was used for antigen retrieval, and freshly prepared PBS containing 0.3% hydrogen peroxide was used to block endogenous peroxidase activity. The intestine tissue sections were subsequently incubated with antibody against ZO-1 (1:500, ab276131, abcam) overnight at 4 °C in a humidified chamber. On the next day, the sections were incubated with a horseradish peroxidase (HRP)-conjugated goat anti-rabbit secondary antibody at 37 °C for 30 min. Three non-consecutive sections were evaluated per mouse (n = 6/group), and five non-overlapping fields per section were examined at 200× magnification. Representative images were selected from anatomically matched fields to illustrate the distribution and staining pattern of ZO-1.

2.11. ELISA

Blood was collected at the experimental endpoint and allowed to clot at room temperature for 30 min. Samples were centrifuged at 3000× g for 10 min at 4 °C, and the serum was collected. Serum COX-2 was measured using a Mouse Cyclooxygenase-2 ELISA Kit (CSB-E12910m, CUSABIO, Wuhan, China). IL-1β, IL-6, and TNF-α were measured using Mouse IL-1β ELISA Kit (RAB0274), Mouse IL-6 ELISA Kit (RAB0308), and Mouse TNF-α ELISA Kit (RAB0477), respectively (Sigma-Aldrich, St. Louis, MO, USA). All assays were

performed according to the manufacturers' instructions. Optical density was measured at 450 nm using a microplate reader.

2.12. Intestinal Transit Time

The intestinal transit time (ITT) was measured as previously described [18]. A total of 200 µL of FITC-dextran (70 kDa, ThermoFisher) with a concentration of 6.25 mg/mL were administered via oral gavage after fasting for 24 h. After 30 min, the mice were sacrificed and the entire gastrointestinal tract was divided into 15 segments (one part of stomach, ten equal parts of small bowel, one part from cecum and three equal parts from the colon). The contents of the gastrointestinal tract were collected in tubes with Krebs–Henseleit buffer solution. Then, the fluorescence intensity of each intestinal segment was examined using a microplate reader (ELX800, BioTek Instruments, Winooski, VT, USA) with an excitation wavelength of 494 nm and emission wavelength of 521 nm.

2.13. Malondialdehyde (MDA), Glutathione (GSH) and Iron Content Assays

At the experimental endpoint, distal ileal tissues were collected and homogenized at 10% (*w*/*v*) in ice-cold PBS. Homogenates were centrifuged at 12,000× *g* for 10 min at 4 °C, and the supernatants were used for biochemical assays. MDA was measured using a Malondialdehyde Assay Kit (TBA method, A003-1-2; Nanjing Jiancheng Bioengineering Institute, Nanjing, China). Reduced GSH was measured using a Reduced Glutathione Assay Kit (A006-1-1; Nanjing Jiancheng Bioengineering Institute). Ferrous iron (Fe^{2+}) was determined using an Iron Assay Kit (ab83366; Abcam, Cambridge, UK). Protein concentrations were measured using a BCA Protein Assay Kit (P0012; Beyotime Biotechnology, Shanghai, China). Biochemical measurements were normalized to total protein concentration. For graphical presentation, normalized values were expressed relative to the mean value of the Sham group, which was defined as 100%.

2.14. Statistical Analysis

Statistical analyses for animal experiments were performed using SPSS 22.0 (IBM Corp., Armonk, NY, USA) and GraphPad Prism 8.0 (GraphPad Software, San Diego, CA, USA). Data are presented as mean ± standard deviation (SD). Prior to parametric testing, normality and homogeneity of variance were assessed. To ensure objectivity, all downstream molecular evaluations (including ELISA, Western blot, and IHC) were performed by investigators blinded to the experimental allocation of the animal groups. For comparisons among three or more groups, one-way ANOVA was applied when assumptions were met, followed by least significant difference (LSD) post hoc testing under equal variances; when variances were unequal, Dunnett's T3 post hoc test was used. For two-group comparisons, Student's *t* test was used when data were normally distributed; otherwise, the Wilcoxon rank-sum test was applied. For non-normally distributed data involving three or more groups, the Kruskal–Wallis test was used with appropriate post hoc multiple comparisons.

Bioinformatic and transcriptomic analyses of public datasets were conducted in the R statistical environment (v4.5.2). Differences in z-scored module scores between groups were assessed using two-sided Student's *t* tests (unpaired for the mouse datasets and paired for the human GSE263125 dataset). When multiple hypothesis testing was involved (e.g., differential expression and pathway analyses), *p* values were adjusted using the Benjamini–Hochberg method to control the false discovery rate (FDR). Unless otherwise specified, all tests were two-sided. A value of $p < 0.05$ (or FDR-adjusted $p < 0.05$ where applicable) was considered statistically significant.

3. Results

3.1. Moxibustion Improves Gastrointestinal Function and Alleviates Intestinal Injury in IM-Induced POI Mice

We first established an IM-induced POI mouse model and applied moxibustion at Shenque (CV8) for 4 weeks according to the experimental scheme (Figure 1A). Histopathological examination showed preserved intestinal architecture in Sham and MOX groups, whereas POI mice exhibited marked mucosal injury and structural disruption; these pathological changes were mitigated in the POI + MOX group (Figure 1B). Consistent with postoperative burden, POI mice displayed reduced body weight gain relative to Sham controls, while moxibustion attenuated the body weight deficit in POI animals (Figure 1C). Functionally, FITC-dextran-based transit analysis demonstrated a pronounced IM-induced delay in gastrointestinal propulsion in POI mice, which was significantly improved by moxibustion, shifting FITC-dextran distribution toward a more distal profile (Figure 1D). Together, these data establish a reproducible protective phenotype of moxibustion in POI and prompted a mechanism-driven analysis to identify IM-triggered molecular programs that could explain the observed functional recovery.

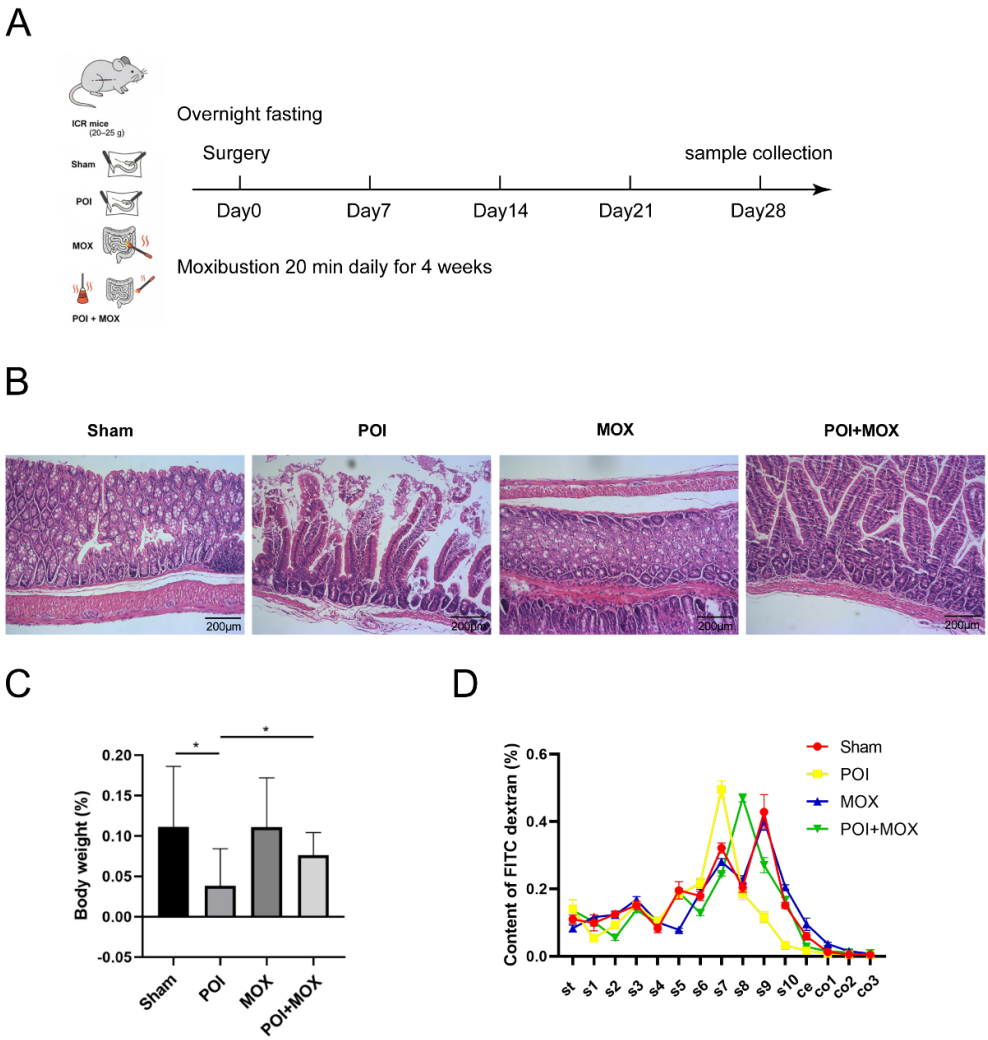


Figure 1. Moxibustion promotes gastrointestinal functional recovery and attenuates intestinal injury in a mouse model of postoperative ileus (POI). (**A**) Experimental scheme and moxibustion intervention timeline. POI was induced by intestinal manipulation (IM), and moxibustion was applied at the Shenque (CV8) acupoint (1.5 cm distance, 20 min/day) for 4 weeks. Samples were collected at Day 28. (**B**) Representative H&E-stained sections of the distal ileum, collected approximately 5 cm proximal

to the ileocecal junction, from Sham, POI, MOX, and POI + MOX mice. All representative panels were selected from anatomically matched regions. Scale bar, 200 μm. (**C**) Percentage change in body weight in each group at the endpoint (n = 6 per group). (**D**) Gastrointestinal transit assessed by FITC-dextran distribution across the stomach (st), ten equal segments of small intestine (s1–s10), cecum (ce), and three equal segments of colon (co1–co3) (n = 6 per group). Data are expressed as mean ± SD. Statistical comparisons were evaluated by one-way ANOVA followed by LSD post hoc test (for equal variances) or Dunnett's T3 test (for unequal variances). * $p < 0.05$; horizontal lines indicate the groups compared (POI vs. Sham and POI + MOX vs. POI).

3.2. IM Time-Course Transcriptomics Nominates Ferroptosis-Associated Remodeling Alongside Inflammation Activation and Barrier Suppression

To define candidate mechanistic axes prior to targeted experiments, we performed a discovery analysis in a public IM time-course dataset (GSE134942). Signature scoring showed a time-dependent increase in the inflammation program from Control to IM3h and IM24h (Figure 2A), accompanied by progressive suppression of barrier/tight-junction signatures (Figure 2B). In parallel, a ferroptosis-associated signature exhibited time-dependent remodeling after IM (Figure 2C). Module-level visualization supported coordinated regulation of representative genes across inflammation, barrier, and ferroptosis-associated modules (Figure 2D). Differential expression analyses (IM3h vs. Control, IM24h vs. Control, and IM24h vs. IM3h) further highlighted key transcripts involved in these axes (Figure 2E–G). Pathway enrichment results consistently prioritized inflammatory response/cytokine signaling and oxidative stress programs together with ferroptosis-associated terms (Figure 2H), while junction/adhesion-related pathways were suppressed, and the overall enrichment landscape was summarized across functional categories (Figure 2I). Collectively, this time-course analysis nominated an IM-associated "inflammation activation-barrier impairment-ferroptosis-associated remodeling" framework, which required external support and experimental confirmation.

3.3. External Transcriptomic Support in an Independent Mouse Cohort and Concordance in Human Surgical Samples

We next evaluated whether the discovery signals generalize across datasets and species. In the independent mouse cohort GSE164909, IM samples showed increased inflammation and ferroptosis-associated signature scores with reduced barrier scores compared with sham surgery (SS) controls (Figure 3A–C), and a module heatmap demonstrated concordant directional regulation of representative genes across these programs (Figure 3D). In the human dataset GSE263125, late-stage intraoperative jejunal muscularis externa samples exhibited higher inflammation and ferroptosis-associated activities and lower barrier-associated signatures relative to early-stage samples (Figure 3E–G). Integrated pathway summaries further supported these group differences (Figure 3H), and the enriched pathway landscape was summarized accordingly (Figure 3I). These external data provide cross-cohort and cross-species support for the IM-associated inflammation-barrier-ferroptosis axis and motivated targeted validation in our POI model.

3.4. Moxibustion Suppresses Systemic Inflammatory Mediators in POI Mice

Guided by the transcriptomic evidence for inflammation activation after IM, we measured circulating inflammatory mediators. POI markedly elevated COX-2 and the pro-inflammatory cytokines IL-1β, IL-6, and TNF-α compared with Sham controls, whereas moxibustion significantly reduced these mediators in POI mice (Figure 4A–D). These results indicate that moxibustion dampens the postoperative inflammatory response in vivo, providing a mechanistic correlate to the functional improvement observed in Figure 1.

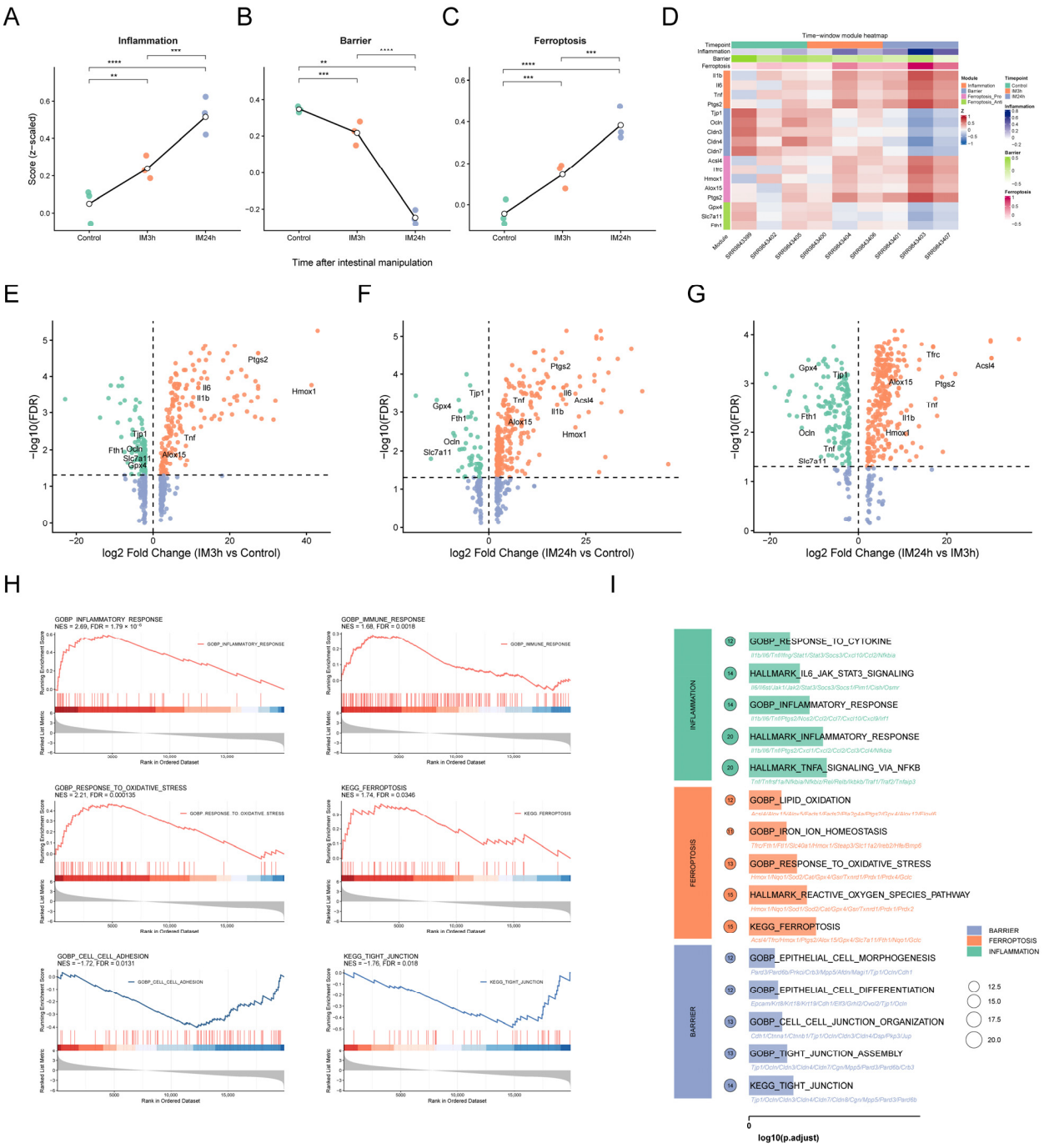


Figure 2. Time-dependent transcriptomic remodeling after intestinal manipulation (IM) in GSE134942. (**A**–**C**) Temporal trends of z-scored signature scores (Inflammation, Barrier, and Ferroptosis) across Control, IM3h, and IM24h. (**D**) Heatmap showing representative genes involved in inflammation, epithelial barrier/tight junction, and ferroptosis modules across the three time points. (**E**–**G**) Volcano plots for differential expression analyses: IM3h vs. Control (**E**), IM24h vs. Control (**F**), and IM24h vs. IM3h (**G**). Key genes related to inflammation (e.g., Il1b/Il6/Tnf/Ptgs2), barrier integrity (e.g., Tjp1/Ocln), and ferroptosis regulation (e.g., Gpx4/Slc7a11/Fth1; Acsl4/Tfrc/Hmox1/Ptgs2/Alox15) are highlighted. (**H**) Representative GSEA enrichment plots illustrating inflammatory response/oxidative stress/ferroptosis and tight-junction-related pathways. (**I**) Dot plot summarizing significantly enriched pathways grouped by inflammation, ferroptosis, and barrier-related programs. In (**E**–**G**), orange and green dots indicate significantly upregulated and downregulated genes (FDR < 0.05), respectively, blue dots indicate genes without significant change, and the horizontal dashed line indicates FDR = 0.05. In (**A**–**C**), ** $p < 0.01$, *** $p < 0.001$, and **** $p < 0.0001$ (two-sided unpaired Student's t test).

https://doi.org/10.3390/biomedicines14112494

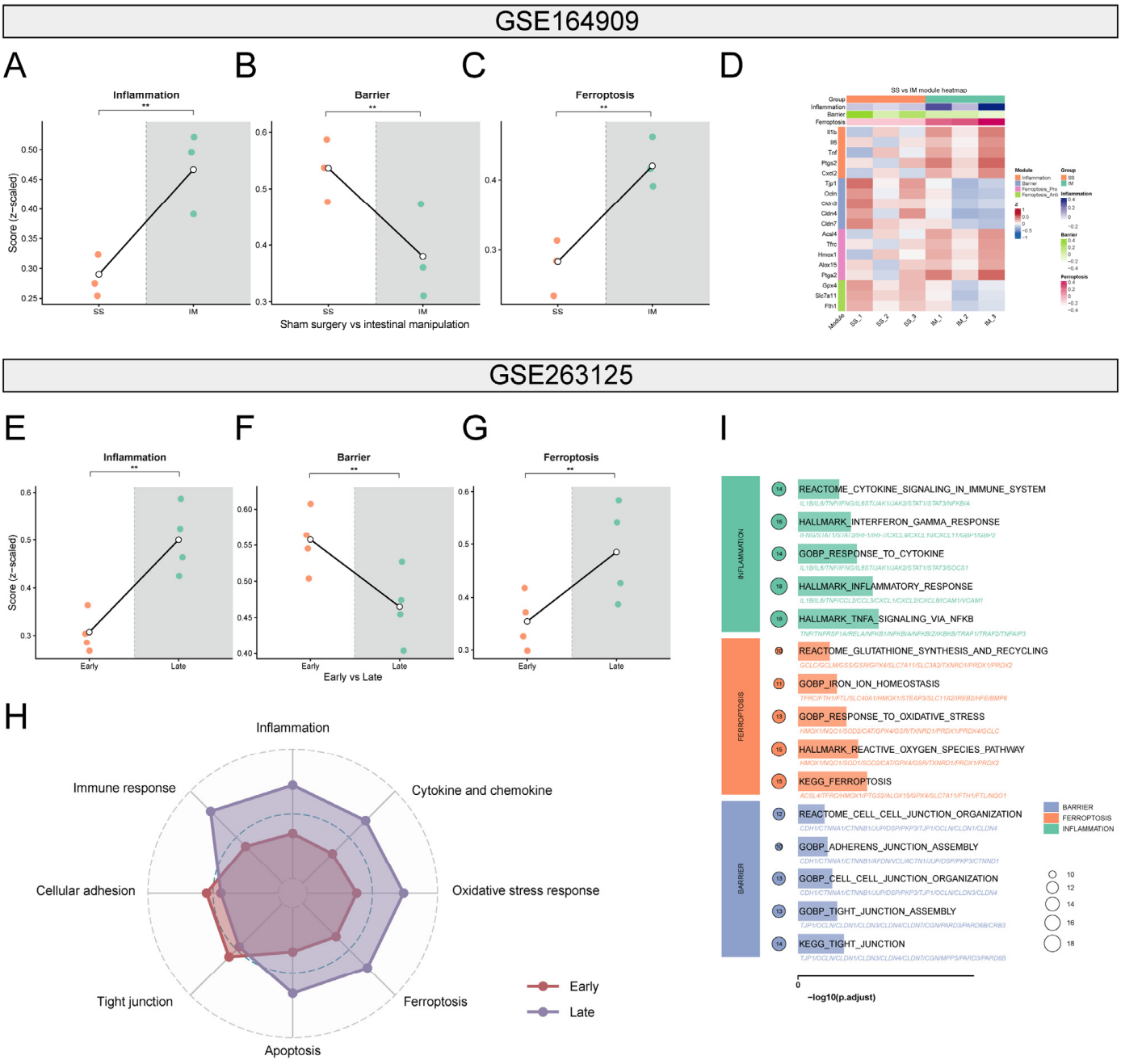


Figure 3. External validation of inflammation activation, barrier impairment, and ferroptosis shift in independent mouse and human transcriptomic cohorts. (**A**–**C**) Z-scored signature scores for inflammation, barrier integrity, and ferroptosis comparing sham surgery (SS) and intestinal manipulation (IM). Each dot represents an individual sample. (**D**) Heatmap of representative genes from the three modules (inflammation, barrier/tight junction, and ferroptosis), showing consistent upregulation of inflammation/ferroptosis-related genes and downregulation of barrier-related genes in IM versus SS. (**E**–**G**) Z-scored signature scores comparing human jejunal muscularis externa samples collected at early versus late intraoperative stages. (**H**) Radar plot summarizing pathway/module activity patterns, highlighting enhanced immune/cytokine response, oxidative stress, and ferroptosis features at the late stage with relative reduction in adhesion/tight junction-related features. (**I**) Dot plot summarizing significantly enriched pathways grouped by inflammation, ferroptosis, and barrier-related programs. ** $p < 0.01$ (two-sided unpaired Student's t test in (**A**–**C**); two-sided paired t test in (**E**–**G**)).

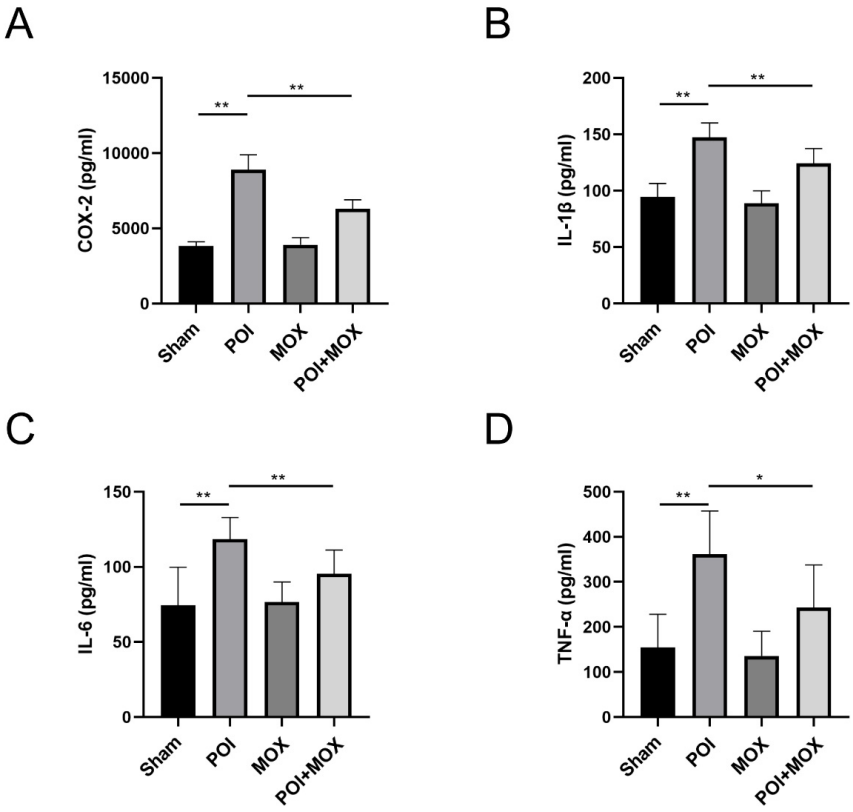


Figure 4. Effect of moxibustion treatment on pro-inflammatory cytokines expression in POI mice. The expression of COX-2 (**A**), IL-1β (**B**), IL-6 (**C**), and TNF-α (**D**) was analyzed by ELISA. * $p < 0.05$, ** $p < 0.01$; horizontal lines indicate the groups compared (POI vs. Sham and POI + MOX vs. POI).

3.5. Moxibustion Restores Intestinal Tight-Junction Markers Associated with Barrier Integrity

Given the consistent barrier suppression across public datasets, we examined canonical tight-junction markers in intestinal tissues. qRT-PCR showed reduced ZO-1 and occludin mRNA levels in POI mice, which were partially restored by moxibustion (Figure 5A,B). Immunoblotting corroborated the same directional changes at the protein level (Figure 5C). Densitometric quantification of independent blots ($n = 6$) confirmed that relative ZO-1 and occludin protein expressions in the POI group were significantly lower than those in the Sham group ($p < 0.01$), and both tight-junction components were significantly upregulated following moxibustion intervention ($p < 0.01$ vs. POI group). Immunohistochemistry further confirmed diminished ZO-1 staining in POI tissues; digital image analysis substantiated that the percentage of ZO-1 positive area was significantly reduced in the POI group compared with the Sham controls ($p < 0.01$), which was significantly rescued in the POI + MOX group ($p < 0.01$ vs. POI) (Figure 5D). These findings experimentally support that moxibustion promotes recovery of barrier-associated components in POI.

3.6. Moxibustion Alleviates Ferroptosis-Related Biochemical Imbalance and Restores GPX4 in POI Mice

Finally, prompted by the discovery and external support for ferroptosis-associated remodeling, we assessed ferroptosis-related markers in intestinal tissues. POI increased lipid peroxidation (MDA) and Fe^{2+} content (Figure 6A,B) and reduced the antioxidant pool GSH (Figure 6C), consistent with a pro-oxidative, iron-dependent stress state. GPX4 protein abundance was also decreased in POI tissues and was upregulated by moxibustion (Figure 6D). Densitometric quantification based on multiple independent biological replicates ($n = 6$) showed that relative GPX4 expression dropped significantly in the POI group relative to Sham ($p < 0.01$), and moxibustion significantly elevated the regulatory protein levels ($p < 0.01$ vs. POI). Together, these results provide experimental evidence

that moxibustion attenuates ferroptosis-associated imbalance in POI, complementing its anti-inflammatory and barrier-restorative effects.

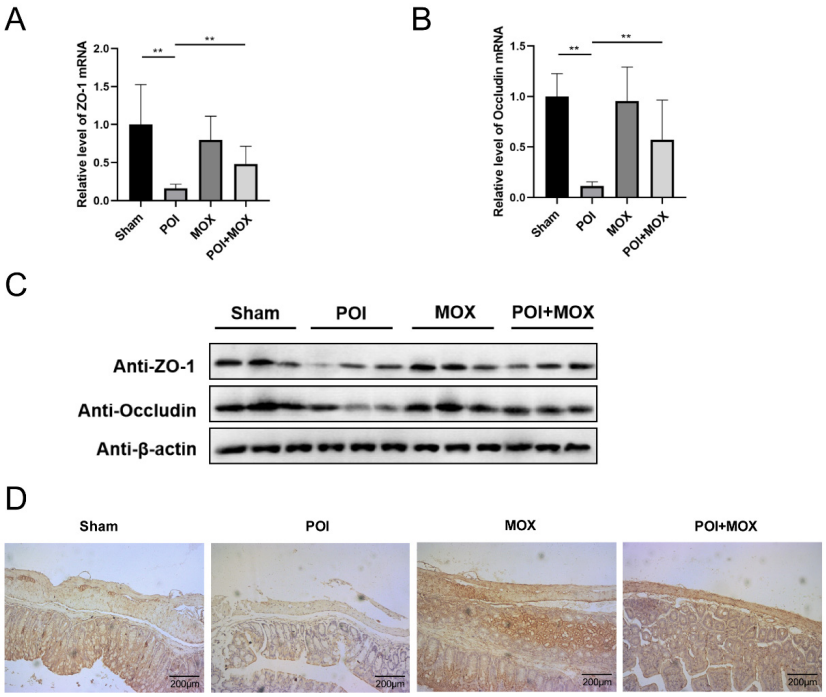


Figure 5. Moxibustion treatment improves intestinal epithelial barrier function in POI mice. (**A**,**B**) qRT-PCR was used to measure the mRNA levels of ZO-1 and occludin in each group. (**C**) Western blotting was used to measure the protein levels of ZO-1 and occludin in each group. (**D**) Immunohistochemical staining was used to examine the expression of ZO-1. ** $p < 0.01$; horizontal lines indicate the groups compared (POI vs. Sham and POI + MOX vs. POI).

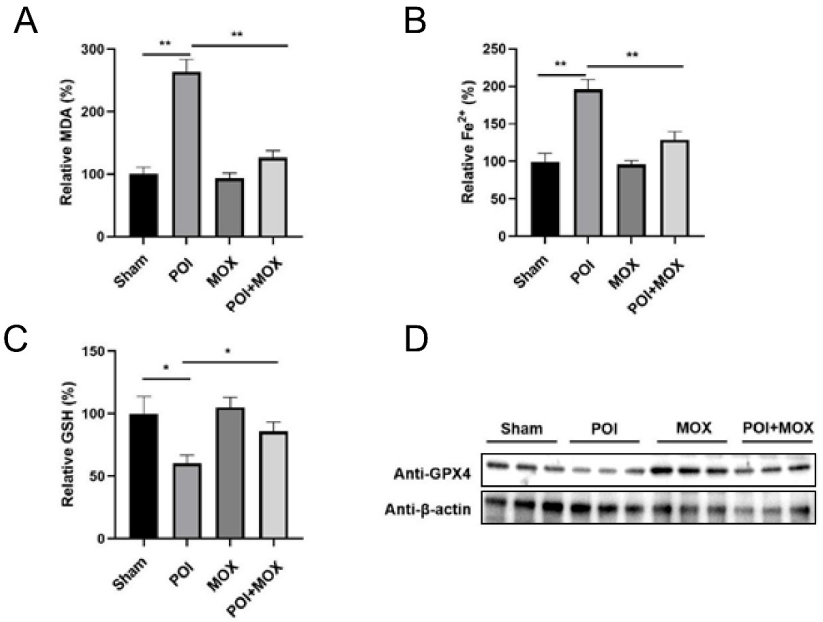


Figure 6. Moxibustion reverses intestinal ferroptosis in POI mice. (**A**) MDA assay kit was used to measure the level of MDA in each group. (**B**) Fe^{2+} assay kit was used to measure the level of Fe^{2+} in each group. (**C**) GSH assay kit was used to measure the level of GSH in each group. (**D**) Western blotting was used to examine the protein level of GPX4 in each group. Data are expressed as mean ± SD. Statistical comparisons were evaluated by one-way ANOVA followed by LSD post hoc test (for equal variances) or Dunnett's T3 test (for unequal variances). * $p < 0.05$, ** $p < 0.01$; horizontal lines indicate the groups compared (POI vs. Sham and POI + MOX vs. POI).

4. Discussion

In this study, we investigated the comprehensive effects of moxibustion at Shenque (CV8) acupoint on IM-induced prolonged intestinal transit time, impaired intestinal epithelial barrier function, inflammation and ferroptosis. Compared with the Sham group, intestinal manipulation in the POI group significantly delayed gastric emptying and small intestinal transit, increased tissue damage and inflammatory cytokines (IL-1β, IL-6 and TNF-α), promoted ferroptosis, and impaired intestinal epithelial barrier function. As expected, moxibustion accelerated intestinal transit, prevented the postoperative increase in IL-1β, IL-6 and TNF-α, alleviated a pro-ferroptotic biochemical state, and improved intestinal epithelial barrier function.

Importantly, to strengthen mechanistic plausibility and avoid post hoc interpretation, we first performed an unbiased transcriptomic exploration using public IM datasets and then validated the nominated programs in independent cohorts and in our own mouse experiments. Specifically, time-course analysis of GSE134942 (Control→IM3h→IM24h) revealed coordinated transcriptional remodeling characterized by increased inflammation signatures, suppressed epithelial barrier/tight-junction programs, and a ferroptosis-associated shift over time. These signatures were reproducible in an independent mouse cohort (GSE164909) and directionally concordant in human intraoperative intestinal samples (GSE263125), supporting the generalizability of the IM-associated inflammation-barrier-ferroptosis axis across datasets and species. This multi-cohort evidence provided a rationale for our targeted experimental validation of inflammatory mediators, tight-junction markers, and ferroptosis-related biochemical and regulatory readouts in the POI model.

The pathogenesis of POI is complicated, and it is generally considered to be regulated by multiple factors containing neurogenic, inflammatory, humoral, and immune [19–21]. During the first 24 h after IM, muscularis macrophages produce the pro-inflammatory cytokines and increase the infiltration of immune cells from the circulation. With more pro-inflammatory macrophages entering the intestine, their released mediators can impair local neuromuscular function, activate neurogenic inhibitory pathways, and inhibit the motility of the intestine [11]. Furthermore, the IM-induced inflammatory responses can increase the permeability of the intestinal epithelium. Consistent with this established framework, our public transcriptomic analyses also highlighted early and sustained activation of inflammatory programs after IM, providing external support for selecting inflammatory cytokines as key readouts in our animal experiments.

Recent studies have demonstrated that ferroptosis is a novel type of regulated cell death linked to inflammatory responses [22,23]. Xu et al. reported the ferroptosis inhibitor Ferrostatin-1 alleviated inflammatory bowel disease via the inhibition of ferroptosis [24]. Further study showed that suppressing ferroptosis ameliorated ulcerative colitis via blocking the Nrf2/HO-1 signaling pathway [25]. Wang et al. demonstrated that a natural ingredient curculigoside inhibited ferroptosis in ulcerative colitis by increasing the ferroptosis negative regulator GPX4 expression [26]. Activation of GPX4 can accelerate the reduction in lipid peroxides and prevent bowel epithelial cells from ferroptosis damage [8,27]. In line with these concepts, our discovery analyses in the IM time-course dataset nominated ferroptosis-associated remodeling as part of the IM response, which was further supported by independent mouse and human transcriptomic cohorts. In the present study, we found that POI model mice suffered from inflammatory responses and exhibited ferroptosis-associated alterations, including reduced GPX4 and an oxidative/iron-dependent biochemical imbalance, whereas moxibustion partially reversed these effects of POI on mice. Notably, given that the public datasets provide association rather than causality, our biochemical (MDA/Fe^{2+}/GSH) and GPX4 measurements serve as targeted

experimental validation supporting a ferroptosis-associated biochemical imbalance in the POI context.

Moxibustion is a traditional thermal intervention in which burning moxa provides localized stimulation at selected acupoints. Experimental evidence suggests that stimulation at Shenque (CV8) can influence gastrointestinal activity and postoperative inflammatory responses. In rats undergoing gastric perforation repair, CV8 moxibustion was associated with improved gastrointestinal function together with reductions in circulating TNF-α and IL-6. These observations provide a rationale for examining CV8 stimulation in postoperative gastrointestinal dysfunction. In the present study, we therefore evaluated moxibustion at CV8 in an IM-induced POI model and observed improvements in gastrointestinal transit accompanied by changes in inflammatory, barrier-associated, and ferroptosis-related readouts [28]. Clinical studies have shown that CV8 is an important acupoint for the treatment of gastrointestinal disorders. CV8 is a point at the mice's navel and has the functions of harmonizing the stomach and intestine. Na-Na Yang et al. have demonstrated that electroacupuncture can suppress intestinal inflammation and promote gastrointestinal motility [11]. Similarly, we found that moxibustion accelerated intestinal transit. However, because neural activity was not directly measured in this study, this interpretation should be considered a plausible hypothesis rather than a demonstrated mechanism, and future work incorporating vagotomy/pharmacological blockade would be required to establish causality.

Most importantly, moxibustion may work by regulating inflammation and ferroptosis. Inflammatory factors are closely related to the incidence and development of POI [29]. Previous studies have demonstrated that the pro-inflammatory factors IL-1β, IL-6 and TNF-α in mice and in human with POI were elevated [4,30–32]. IL-1β deficiency protects mice from POI by accelerating gastrointestinal transit [32]. In our study, compared with the Sham group, the levels of IL-1β, IL-6 and TNF-α increased in the serum of the POI group, indicating that the POI model caused the aggravation of inflammation. Simultaneously, we found that moxibustion inhibited the IL-1β, IL-6 and TNF-α expression, meaning that moxibustion treatment regulated the inflammation of POI. In addition, cyclooxygenase (COX)-2 is a major cause of gastric and duodenal ulceration and identified as a key enzyme in POI [33], our result demonstrated that moxibustion reversed IM-induced increases in COX-2. Although few studies demonstrate that POI is connected with ferroptosis, recent studies showed that moxibustion protected Dopaminergic Neurons in Parkinson's Disease by anti-ferroptosis mechanisms [34]. Extending these observations to the POI setting, our multi-cohort transcriptomic analyses nominated ferroptosis-associated remodeling after IM, and our in vivo experiments further demonstrated that moxibustion restored GPX4 and improved ferroptosis-related biochemical markers, supporting ferroptosis modulation as a component of its protective effects.

Simultaneously, in the present study, compared with Sham group, the levels of ZO-1 and occludin were decreased in POI group; then moxibustion treatment partly reversed the expression of ZO-1 and occludin in POI model mice. As tight junction proteins, ZO-1 and occludin play important roles in inflammatory bowel disease, including ulcerative colitis and Crohn's disease [35–37]. Similar to inflammatory bowel disease, POI is also associated with high levels of pro-inflammatory factors and ferroptosis-associated oxidative stress, which may affect the intestinal barrier function. Consistent with the public IM transcriptomic evidence showing suppression of barrier/tight-junction programs after IM, our experimental data provide tissue-level confirmation that moxibustion supports barrier recovery in POI mice. Taken together, these findings support a coherent mechanistic model in which IM triggers a coupled inflammatory response, barrier disruption, and ferroptosis-associated remodeling, and moxibustion promotes functional recovery at least in part by

counteracting these programs. These parallel changes suggest a potential feedback loop where IM-induced inflammation triggers ROS-mediated lipid peroxidation/ferroptosis, which secondarily breaks down tight junction assemblies, representing an interactive axis open for future hierarchical dissection.

Limitations: It should be noted that the current evidence showing alterations in MDA, Fe^{2+}, GSH, and GPX4 remains correlative and descriptive of a ferroptosis-associated state rather than providing direct causal proof, as specific ferroptosis inhibitors or genetic knockout models were not employed to perform functional rescue. A further limitation is that the therapeutic efficacy of moxibustion was directly evaluated only in ICR mice. Although the major IM-associated transcriptional changes were reproduced in independent BL6/C57BL/6 datasets, these public cohorts do not establish strain-independent responsiveness to moxibustion. Direct comparisons among ICR, C57BL/6, and BALB/c mice will therefore be informative in future studies.

5. Conclusions

In summary, in a mouse model of POI induced by IM, moxibustion at Shenque (CV8) acupoint exerted a prokinetic effect on intestinal transit, prevented the postoperative increase in pro-inflammatory cytokines and ferroptosis, and improved intestinal epithelial barrier function. Further studies in POI model with different IM severity and moxibustion treatment should enable to find the mechanistic insights in moxibustion-mediated amelioration of POI.

Supplementary Materials: The following supporting information can be downloaded at: https://www.mdpi.com/article/10.3390/biomedicines14112494/s1, Figure S1: Amplification and melting-curve analysis of qRT-PCR primers; Table S1: Gene composition of the Inflammation, Ferroptosis, and Barrier modules.

Author Contributions: F.Z. and C.K. were responsible for the conception and design of the study. F.M. and S.Z. contributed equally to this work and share first authorship; they were responsible for data acquisition and performed the transcriptomic analyses of public GEO datasets for multi-cohort validation. Y.Z. and J.S. assisted with data collection and experimental procedures. F.M., S.Z. and Y.Z. performed the formal analysis. F.M. drafted the manuscript. F.Z. and C.K. revised and commented the draft. All authors have read and agreed to the published version of the manuscript.

Funding: This project was funded by Young Talents Program of Changzhou Commission of Health (support number CZQM2020098). The funder has no role/influence in this study.

Institutional Review Board Statement: Animal welfare and experimental procedures were approved by the Laboratory Animal Welfare and Ethics Committee of Nanjing Medical University (Approval No. IACUC-2211079, Approval date 1 December 2022).

Informed Consent Statement: Not applicable.

Data Availability Statement: The data generated and/or analyzed in the current study are available from the corresponding author upon reasonable request. Publicly available transcriptomic datasets analyzed in this study were obtained from the NCBI Gene Expression Omnibus (GEO) under accession numbers GSE134942, GSE164909, and GSE263125.

Acknowledgments: We thank Xiaolan Ding (Changzhou Medical Center, Nanjing Medical University) for her valuable assistance. We also acknowledge the Gene Expression Omnibus (GEO) repository and the investigators who generated and shared the public datasets used in this study, including GSE134942, GSE164909, and GSE263125.

Conflicts of Interest: The authors declare no conflicts of interest.

References

1. Mattei, P.; Rombeau, J.L. Review of the pathophysiology and management of postoperative ileus. *World J. Surg.* **2006**, *30*, 1382–1391. [CrossRef]
2. Buscail, E.; Deraison, C. Postoperative ileus: A pharmacological perspective. *Br. J. Pharmacol.* **2022**, *179*, 3283–3305. [CrossRef]
3. Iyer, S.; Saunders, W.B.; Stemkowski, S. Economic burden of postoperative ileus associated with colectomy in the United States. *J. Manag. Care Pharm.* **2009**, *15*, 485–494. [CrossRef]
4. Snoek, S.A.; Dhawan, S.; van Bree, S.H.; Cailotto, C.; van Diest, S.A.; Duarte, J.M.; Stanisor, O.I.; Hilbers, F.W.; Nijhuis, L.; Koeman, A.; et al. Mast cells trigger epithelial barrier dysfunction, bacterial translocation and postoperative ileus in a mouse model. *Neurogastroenterol. Motil.* **2012**, *24*, 172–184.e191. [CrossRef]
5. Stein, K.; Hieggelke, L.; Schneiker, B.; Lysson, M.; Stoffels, B.; Nuding, S.; Wehkamp, J.; Kikhney, J.; Moter, A.; Kalff, J.C.; et al. Intestinal manipulation affects mucosal antimicrobial defense in a mouse model of postoperative ileus. *PLoS ONE* **2018**, *13*, e0195516. [CrossRef]
6. Wu, Y.T.; Zhong, L.S.; Huang, C.; Guo, Y.Y.; Jin, F.J.; Hu, Y.Z.; Zhao, Z.B.; Ren, Z.; Wang, Y.F. β-Caryophyllene Acts as a Ferroptosis Inhibitor to Ameliorate Experimental Colitis. *Int. J. Mol. Sci.* **2022**, *23*, 16055. [CrossRef]
7. Xu, X.; Ye, H.; Ren, Q.; Shao, X.; Wang, J.; Shi, Y.; Du, Y. Ferroptosis as a mediator of gut microbiota-driven inflammatory bowel disease: Evidence from genetic analyses. *Medicine* **2026**, *105*, e47614. [CrossRef]
8. Li, J.; Tian, X.; Liu, J.; Mo, Y.; Guo, X.; Qiu, Y.; Liu, Y.; Ma, X.; Wang, Y.; Xiong, Y. Therapeutic material basis and underling mechanisms of Shaoyao Decoction-exerted alleviation effects of colitis based on GPX4-regulated ferroptosis in epithelial cells. *Chin. Med.* **2022**, *17*, 96. [CrossRef]
9. Bresser, M.; Siemens, K.D.; Schneider, L.; Lunnebach, J.E.; Leven, P.; Glowka, T.R.; Oberlander, K.; De Domenico, E.; Schultze, J.L.; Schmidt, J.; et al. Macrophage-induced enteric neurodegeneration leads to motility impairment during gut inflammation. *EMBO Mol. Med.* **2025**, *17*, 301–335. [CrossRef]
10. Schneider, R.; Leven, P.; Glowka, T.; Kuzmanov, I.; Lysson, M.; Schneiker, B.; Miesen, A.; Baqi, Y.; Spanier, C.; Grants, I.; et al. A novel P2X2-dependent purinergic mechanism of enteric gliosis in intestinal inflammation. *EMBO Mol. Med.* **2021**, *13*, e12724. [CrossRef]
11. Yang, N.N.; Yang, J.W.; Ye, Y.; Huang, J.; Wang, L.; Wang, Y.; Su, X.T.; Lin, Y.; Yu, F.T.; Ma, S.M.; et al. Electroacupuncture ameliorates intestinal inflammation by activating α7nAChR-mediated JAK2/STAT3 signaling pathway in postoperative ileus. *Theranostics* **2021**, *11*, 4078–4089. [CrossRef]
12. Shi, Y.; Zheng, Y.; Xu, J.; Ding, B.; Shou, Q.; Chen, G.; Liu, T.; Sun, Q.; Xu, X. Gastrointestinal Motility and Gut Hormone Secretion in response to Shenhuang Plaster in a Postoperative Ileus Rat Model. *Evid.-Based Complement. Altern. Med.* **2021**, *2021*, 8859579. [CrossRef]
13. Kuge, H.; Mori, H.; Morisawa, T.; Hanyu, K.; Miyazaki, J.; Watanabe, M.; Tanaka, T.H. Effect of Different Dosages of ST36 Indirect Moxibustion on the Skin Temperature of the Lower Legs and Feet. *Medicines* **2018**, *5*, 57. [CrossRef]
14. Li, H.X.; Shi, L.; Liang, S.J.; Fang, C.C.; Xu, Q.Q.; Lu, G.; Wang, Q.; Cheng, J.; Shen, J.; Shen, M.H. Moxibustion alleviates decreased ovarian reserve in rats by restoring the PI3K/AKT signaling pathway. *J. Integr. Med.* **2022**, *20*, 163–172. [CrossRef]
15. Zhao, M.; Weng, Z.; Huang, Y.; Zheng, H.; Han, D.; Shen, J.; Huang, R.; Liu, H.; Wu, L. Herb-Partitioned Moxibustion Improves Crohn's Disease-Associated Intestinal Fibrosis by Suppressing the RhoA/ROCK1/MLC Pathway. *Evid.-Based Complement. Altern. Med.* **2021**, *2021*, 2247953. [CrossRef]
16. Zhang, X.; Guo, Y.; Shi, J.; Zang, Q.; Li, Y. Exclusive Effects of Moxibustion on Gut Microbiota: Protocol for a Focused Systematic Review and Meta-Analysis. *JMIR Res. Protoc.* **2025**, *14*, e73317. [CrossRef]
17. Elfar, W.; Gurjar, A.A.; Talukder, M.A.H.; Noble, M.; Di Lorenzo, C.; Elfar, J. Erythropoietin promotes functional recovery in a mouse model of postoperative ileus. *Neurogastroenterol. Motil.* **2021**, *33*, e14049. [CrossRef]
18. Vilz, T.O.; Overhaus, M.; Stoffels, B.; Websky, M.; Kalff, J.C.; Wehner, S. Functional assessment of intestinal motility and gut wall inflammation in rodents: Analyses in a standardized model of intestinal manipulation. *J. Vis. Exp.* **2012**, *11*, 4086. [CrossRef]
19. Bauer, A.J.; Boeckxstaens, G.E. Mechanisms of postoperative ileus. *Neurogastroenterol. Motil.* **2004**, *16*, 54–60. [CrossRef]
20. Bragg, D.; El-Sharkawy, A.M.; Psaltis, E.; Maxwell-Armstrong, C.A.; Lobo, D.N. Postoperative ileus: Recent developments in pathophysiology and management. *Clin. Nutr.* **2015**, *34*, 367–376. [CrossRef]
21. Venara, A.; Neunlist, M.; Slim, K.; Barbieux, J.; Colas, P.A.; Hamy, A.; Meurette, G. Postoperative ileus: Pathophysiology, incidence, and prevention. *J. Visc. Surg.* **2016**, *153*, 439–446. [CrossRef]
22. Cao, L.; Qin, R.; Liu, J. Farnesoid X receptor protects against lipopolysaccharide-induced endometritis by inhibiting ferroptosis and inflammatory response. *Int. Immunopharmacol.* **2023**, *118*, 110080. [CrossRef]
23. Shi, Z.; Zhang, S.; Zhai, H.; Wu, Q.; Li, Y.; Xu, H.; Zhang, S. The interplay mechanisms between gut microbiota and ferroptosis in inflammatory bowel disease. *Front. Immunol.* **2026**, *17*, 1753617. [CrossRef]
24. Xu, J.; Liu, S.; Cui, Z.; Wang, X.; Ning, T.; Wang, T.; Zhang, N.; Xie, S.; Min, L.; Zhang, S.; et al. Ferrostatin-1 alleviated TNBS induced colitis via the inhibition of ferroptosis. *Biochem. Biophys. Res. Commun.* **2021**, *573*, 48–54. [CrossRef]

25. Chen, Y.; Zhang, P.; Chen, W.; Chen, G. Ferroptosis mediated DSS-induced ulcerative colitis associated with Nrf2/HO-1 signaling pathway. *Immunol. Lett.* **2020**, *225*, 9–15. [CrossRef]
26. Wang, S.; Liu, W.; Wang, J.; Bai, X. Curculigoside inhibits ferroptosis in ulcerative colitis through the induction of GPX4. *Life Sci.* **2020**, *259*, 118356. [CrossRef]
27. Yue, Z.; Yuan, Y.; Zhou, Q.; Sheng, J.; Xin, L. Ferroptosis and its current progress in gastric cancer. *Front. Cell Dev. Biol.* **2024**, *12*, 1289335. [CrossRef]
28. Shen, J.; Ai, B.; Shen, M. Effectiveness of Mild Moxibustion for Sub-Health Conditions in Pre- and Post-Menopausal Women: A Randomized Controlled Clinical Trial. *Med. Sci. Monit.* **2018**, *24*, 2907–2911. [CrossRef]
29. Zou, K.; Chen, W.; Dai, J.; Mo, P.; Yu, C.; Xu, J.; Wu, S.; Zhuo, R.; Su, G. Steroid Receptor Coactivator-3 Is Required for Inhibition of the Intestinal Muscularis Inflammatory Response of Postoperative Ileus in Mice. *Inflammation* **2021**, *44*, 1145–1159. [CrossRef]
30. Kalff, J.C.; Turler, A.; Schwarz, N.T.; Schraut, W.H.; Lee, K.K.; Tweardy, D.J.; Billiar, T.R.; Simmons, R.L.; Bauer, A.J. Intra-abdominal activation of a local inflammatory response within the human muscularis externa during laparotomy. *Ann. Surg.* **2003**, *237*, 301–315. [CrossRef]
31. Stoffels, B.; Hupa, K.J.; Snoek, S.A.; van Bree, S.; Stein, K.; Schwandt, T.; Vilz, T.O.; Lysson, M.; Veer, C.V.; Kummer, M.P.; et al. Postoperative ileus involves interleukin-1 receptor signaling in enteric glia. *Gastroenterology* **2014**, *146*, 176–187 e171. [CrossRef]
32. Hupa, K.J.; Stein, K.; Schneider, R.; Lysson, M.; Schneiker, B.; Hornung, V.; Latz, E.; Iwakura, Y.; Kalff, J.C.; Wehner, S. AIM2 inflammasome-derived IL-1β induces postoperative ileus in mice. *Sci. Rep.* **2019**, *9*, 10602. [CrossRef]
33. Van Dingenen, J.; Pieters, L.; Vral, A.; Lefebvre, R.A. The H_2S-Releasing Naproxen Derivative ATB-346 and the Slow-Release H_2S Donor GYY4137 Reduce Intestinal Inflammation and Restore Transit in Postoperative Ileus. *Front. Pharmacol.* **2019**, *10*, 116. [CrossRef]
34. Huang, Z.; Si, W.; Li, X.; Ye, S.; Liu, X.; Ji, Y.; Hao, X.; Chen, D.; Zhu, M. Moxibustion Protects Dopaminergic Neurons in Parkinson's Disease through Antiferroptosis. *Evid.-Based Complement. Altern. Med.* **2021**, *2021*, 6668249. [CrossRef]
35. Rui, X.; Li, J.; Yang, Y.; Xu, L.; Liu, Y.; Zhang, M.; Yin, D. Painong San, a Traditional Chinese Compound Herbal Medicine, Restores Colon Barrier Function on DSS-Induced Colitis in Mice. *Evid.-Based Complement. Altern. Med.* **2021**, *2021*, 2810915. [CrossRef]
36. Zhu, X.; Yang, Y.; Gao, W.; Jiang, B.; Shi, L. Capparis spinosa Alleviates DSS-Induced Ulcerative Colitis via Regulation of the Gut Microbiota and Oxidative Stress. *Evid.-Based Complement. Altern. Med.* **2021**, *2021*, 1227876. [CrossRef]
37. Ding, Y.X.; Chen, L.L.; Li, K.W.; Zou, L.; Liao, L.M.; Han, X.Y.; OuYang, J.; Wu, Y.P.; Zhang, W.D.; Chu, H.R. Assessing the impact of moxibustion on colonic mucosal integrity and gut microbiota in a rat model of cerebral ischemic stroke: Insights from the "brain-gut axis" theory. *Front. Neurol.* **2025**, *16*, 1450868. [CrossRef]

Disclaimer/Publisher's Note: The statements, opinions and data contained in all publications are solely those of the individual author(s) and contributor(s) and not of MDPI and/or the editor(s). MDPI and/or the editor(s) disclaim responsibility for any injury to people or property resulting from any ideas, methods, instructions or products referred to in the content.